forests

MDPI

Article

A Clustering–Connection Algorithm for Coarse Root System Architecture Reconstruction Based on Ground-Penetrating Radar

Yuntong Liu, Luyun Zhang, Xihong Cui *, Xuehong Chen, Huaxiang Yin and Xin Cao

State Key Laboratory of Remote Sensing and Digital Earth, Faculty of Geographical Science, Beijing Normal University, Beijing 100875, China; lyuntong@mail.bnu.edu.cn (Y.L.); luyun@mail.bnu.edu.cn (L.Z.); chenxuehong@bnu.edu.cn (X.C.); yinhuaxiang@mail.bnu.edu.cn (H.Y.); caoxin@bnu.edu.cn (X.C.)

* Correspondence: cuixihong@bnu.edu.cn or cuixihong@mail.bnu.edu.cn

Abstract: Root system architecture (RSA), a critical attribute of plant roots, necessitates in situ reconstruction to advance the understanding of the subsurface plant root system. Ground Penetrating Radar (GPR), a non-invasive geophysical technique for in situ detection, has demonstrated success in plant RSA reconstruction. However, existing GPR-based methods have limitations, including their applicability to a specific survey line arrangement, reliance on root attribute information, numerous parameter settings, and a focus on incomplete root systems. To address these issues, a new clustering–connection (CC) method is proposed, which considers the root extension direction and growth characteristics for RSA reconstruction. Experimental results show that the CC method achieves accuracy rates of 93.38% and 88.17% for circular and grid survey line arrangements in simulated data, with deviation rates of 3.23% and 9.17% for root lengths. The method also delivered effective results with measured data. This study overcomes the limitations of survey lines and numerous parameters, enabling effective RSA reconstruction. It provides a methodological foundation and reference data for using GPR in urban tree root monitoring by estimating ecological parameters in the forest subsurface and analyzing root distribution patterns in deep-rooted and shallow-rooted plants.

Keywords: ground-penetrating radar; non-invasive; in situ detection; root system architecture reconstruction; clustering–connection

check for updates

Received: 27 January 2025
Revised: 1 March 2025
Accepted: 6 March 2025
Published: 8 March 2025

Citation: Liu, Y.; Zhang, L.; Cui, X.; Chen, X.; Yin, H.; Cao, X. A Clustering–Connection Algorithm for Coarse Root System Architecture Reconstruction Based on Ground-Penetrating Radar. *Forests* **2025**, *16*, 475. https://doi.org/10.3390/f16030475

1. Introduction

The plant root system, as a key organ of the plant, not only plays a crucial role in the uptake and storage of water and nutrients but also has an indispensable function in plant anchorage and support [1]. RSA is closely related to the spatial structure and morphological characteristics of the root system, which determines the important functions of the root system [2]. RSA is the result of a combination of intrinsic genetic factors and extrinsic environmental factors, which can reflect the growth strategy of plants under specific environmental conditions [3]. Therefore, the study of RSA is scientifically important for the in-depth understanding of root–soil or root–environment interactions [4].

Although RSA plays an important role in plant root studies, rapid access to RSA from single plants is still challenging, especially for larger woody plants. The main reason for this is that the plant root system is deeply buried in the soil, its observation and measurement are much less intuitive than that of the above-ground parts of the plant, such as the trunk and crown.

Conventional destructive techniques such as drilling [5] and profiling [6] can obtain accurate information about the parts of the root system. They are not only time-consuming and labor-intensive but also have the potential to disrupt the natural RSA during the observation process [7]. With the advancement of geophysical and photogrammetric techniques, root scanning techniques based on image analysis [8], X-ray tomography [9], nuclear magnetic resonance tomography [10,11], 3D laser scanning point cloud data reconstruction [12], minirhizotron [13], and GPR, etc., are gradually being applied in RSA research. Compared to traditional excavation measurements, laboratory-based measurements now include root scanning, X-ray tomography, nuclear magnetic resonance tomography, and 3D laser scanning. Their advantage is their ability to obtain more accurate information about the root system. But they require root excavation (Root scanning, 3D laser scanning) or are limited to detecting small fine roots (X-ray tomography, minimum effective identified root diameter 100 μm, nuclear magnetic resonance tomography, minimum effective identified root diameter 200 μm). Methods that enable in situ measurements in the field include minirhizotron and GPR. The minirhizotron method is based on the application of transparent tubes, located in a plant's root zone [13]. Continuous root image acquisition and analysis using minirhizotron. This method has been widely used in plant root studies [14], but it has the disadvantages of a high deployment workload and limited coverage in the field. In contrast, GPR offers the advantages of in situ, non-destructive field detection, and the ability to detect coarse roots.

GPR employs electromagnetic waves transmitted by an antenna to penetrate subsurface materials. Using the difference in dielectric permittivity between the root system and the surrounding soil medium due to the difference in water content, the electromagnetic wave will be reflected when it comes into contact with the plant root system, forming a recognizable signal [15–17]. The B-scan images acquired by GPR reflect the subsurface profile through which GPR passes, and the plant root system is usually characterized by a hyperbola in the B-scan images. The apex of the hyperbola considered to be the location of the root, i.e., the root point. The set of all root points of a plant under GPR detection is defined as the root point cloud data. By analyzing the root point cloud data, relevant information such as the location and properties of the roots can be obtained and further used in RSA reconstruction. Therefore, GPR is mainly applied to the detection of coarse roots (root diameter > 2 mm) in plants [18].

The research on RSA in plants can be traced back to 1999, when Cermak et al. used a manual visual interpretation of multiple radar images and manually connected them to draw a three-view diagram of RSA [19,20]. Although some studies have directly reconstructed root configurations using C-scan images combined with B-scan images [21,22], they suffer from the drawbacks of relatively poor accuracy and a need for visual interpretation. Therefore, the problem of reconstructing the RSA of coarse roots based on GPR can be transformed into the problem of point-to-point connectivity in root point cloud data. Wu et al. proposed a retrospective search-window method based on the arrangement of concentric circles of survey lines [23], which takes into account the uniqueness of the outward-to-inward connectivity of the root growth characteristics, the consistency in root growth direction, and the diameter-related attributes of the root. However, this method relies on circular survey line information, and data from non-circular lines is incompatible. Ohashi et al. proposed a method for RSA reconstruction based on weighted inter-root point distances and cosine angles [24]. It requires the root diameter for evaluation and extensive experimentation to determine the parameter weight. Aboudourib et al. proposed a simple framework from root point identification to the reconstruction of RSA [25]. Xiao et al. obtained the optimal RSA by restricting the candidate range through the distance between root points, and at the same time, considered the information on root diameter, root depth, and root extension angle weighted between root points [26]. It also requires determining and setting the weights of the three parameters after numerous trials. Fan et al.

proposed a reconstruction method based on the threshold limitation of the deviation angle between root points by thresholding multiple angle attributes (azimuth, pitch, and deviation) between root points [27]. It faces challenges in determining the deviation angle threshold and the potential for numerous unconnected root points. Luo et al. proposed a reconstruction method based on the horizontal direction angle clustering of roots between B-scan slices by restricting the horizontal direction angle attribute and distance attribute of root points, which can effectively deal with the case of multi-branching of root systems [28]. Two dual-polarized antennas are required to obtain the horizontal angle information of the root point, although they can only access a portion of the root system.

In conclusion, there exist the following main problems in the current research on the 3D RSA reconstruction based on GPR: (1) The existing methods are mostly applicable to specific survey line arrangement. (2) Existing methods are more dependent on the root attribute (root diameter, root horizontal direction angle), and the reconstruction effect is not sufficient when the root attribute information is incomplete. (3) Existing methods require extensive experimentation to determine parameters or weighting coefficients. Therefore, this study aims to address the limitations of the existing GPR-based RSA reconstruction methods in terms of survey line applicability, strong dependence on root attributes, and complexity of parameter settings.

The innovation of this study lies in the proposal of a new clustering–connection (CC) method, which enhances the radial growth characteristics of roots through feature coordinate transformation. Starting with the complete root system, the method first clusters and then connects the roots, achieving the 3D reconstruction of the entire RSA without requiring a specific survey line arrangement. Compared to existing methods, the CC method adapts to various survey line arrangements, reduces reliance on root attribute information, and allows for effective root system reconstruction with simple parameter settings. Furthermore, we experimentally validated the method's effectiveness using both simulated and measured data, demonstrating its applicability and robustness under different survey line arrangements. This method not only improves the accuracy of RSA reconstruction but also provides a new methodological foundation and reference data for urban tree root monitoring, ecological parameter estimation in forest subsurfaces, and analysis of root distribution patterns in deep-rooted and shallow-rooted plants.

2. Materials and Methods

2.1. Research Data

2.1.1. Field Measurement Data

The field experimental site was located in a grassland in a prohibited pasture near Xilinhot City (43°55′01″ N, 116°12′24″ E), Xilingol League, Inner Mongolia Autonomous Region (shown in Figure 1a). The area is located in a temperate semi-arid continental climate zone, characterized by a multi-year average temperature of 3.9 °C, an annual precipitation range of 210–344 mm, and the soil mainly being sand (~80% sand and ~20% silt and clay). It lies within the low mountainous and hilly region of the Mongolian Plateau, featuring relatively flat terrain and a uniform soil texture. The vegetation type is grassland shrubs dominated by the *Caragana microphylla* Lam. (*C. microphylla*). The field measurement experiment was conducted in July 2018, during peak vegetation growth. The significant difference between the root water content and soil water content during this time facilitates the acquisition of ideal GPR signal data.

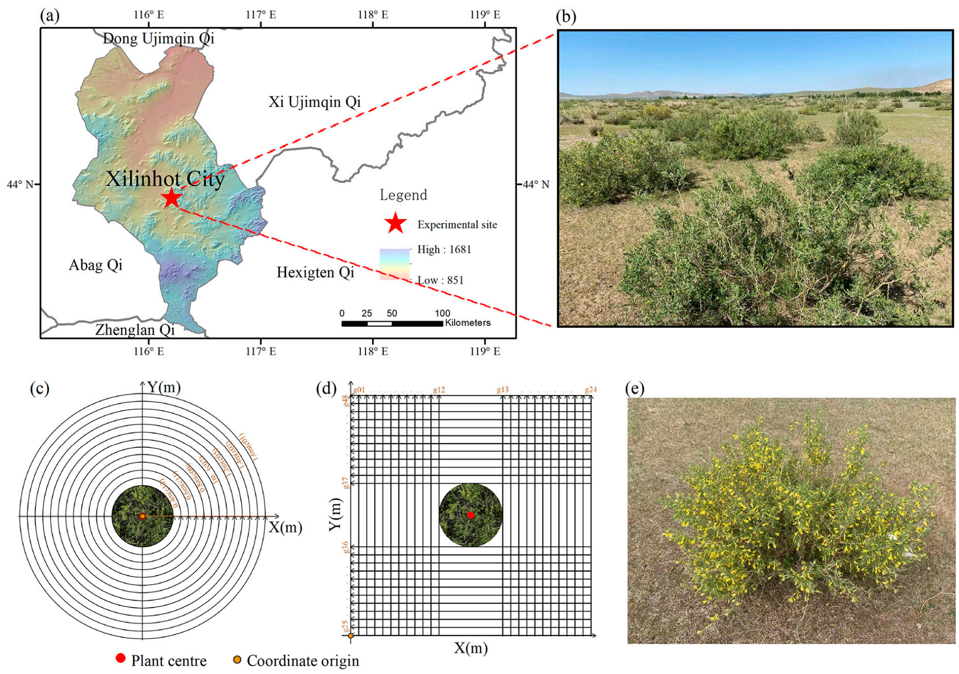

Figure 1. Map of the experimental site and site layout, (**a**) location of the experimental site. (**b**) Landscape of the experimental site. (**c**) Schematic diagrams of the circular survey line layout. (**d**) Schematic diagrams of the grid survey line layout. (**e**) Single plant experiments of *C. microphylla*.

The IDS GPR system (RIS MF Hi-Mod, Ingegneria Dei Sistemi Inc., Pisa, Italy) with a 900 MHz antenna was used to detect the dominant shrub *C. microphylla* in both circular and grid survey line layouts. Before measurement, a metal plate was pre-buried at a depth of 0.3 m under the ground near the root measurement area. The metal plate was detected using GPR during the root system measurement. The orange dots in Figure 1c,d denote the coordinate origin of the current survey line arrangement, with subsequent root point coordinates calculated relative to this origin. Red dots in Figure 1c,d denote the center of the plant, which was an important reference for the GPR measurements. The circular survey line layout is centered on the plant center, with 0.4 m as the starting radius and 1.6 m as the outermost radius. The interval between survey lines is 0.1 m, with equal intervals of incremental arrangement, and a total of 13 survey lines were obtained (shown in Figure 1c). The grid survey line layout is centered on the plant, forming a square measurement site with dimensions of 3 × 3 m. The measurement lines are spaced at intervals of 0.1 m, except within a 0.4 m radius from the plant center, where no measurement lines are placed. The layout features equally spaced survey lines arranged sequentially in both horizontal and vertical directions, with 24 lines in each direction, resulting in a total of 48 measurement lines (shown in Figure 1d). We sprinkled white flour along the laid-out measuring line to help guide the GPR measurements along the flour markings. All lines were measured in the direction indicated by the arrows using GPR. After completing the two survey line measurements, the shrub's root system was excavated for subsequent validation. The main root system was labeled with an eco-friendly dye and photographed for record.

2.1.2. Simulated Root System Data

To quantitatively evaluate the effectiveness of the reconstruction algorithm proposed in this paper, the morphological map of the shrub root system, obtained through an in situ manual excavation within a 70 m^2 area in a prior study [29], was selected as the foundation for the simulation data. The most definitive map of the root system morphology of a single Arctostaphylos pungens was selected for the simulation of GPR measurement data. The presence of granite under 0.6 m of the experimental area prevented root growth. In light of these observations, the root depth range of the simulated data in this study was set to 0–0.6 m. As the GPR was capable of identifying coarse roots with a diameter greater than 2 mm [30], the fine roots were removed and modified in the selected root morphology maps. Subsequently, circular and grid survey lines commonly used in GPR were simulated, and root points were sampled from the 2D image of the root system. The intersection points of each line with the root were extracted to simulate the root point cloud data obtained from the GPR measurements presented in Figure 2a. Green and orange are grid and circular samples, respectively. The depth of each sampled root point was assigned according to the root branch it belonged to and the distance from the root point to the center of the plant, the further the distance, the deeper the root. The distance of root point *i* from the shrub's center and its corresponding depth are determined using Equations (1) and (2):

$$r_i = \sqrt{(x_i - x_c)^2 + (y_i - y_c)^2}, \tag{1}$$

$$deep_i = \frac{(deep_{max} - deep_{min}) \times (r_i - r_{min})}{(r_{max} - r_{min})} + deep_{min}, \tag{2}$$

where $(x_c,\ y_c)$ is the position of the plant center, $(x_i,\ y_i)$ is the position of root point *i*, r_i denotes the distance of root point *i* from the plant center in the x-y plane, $deep_i$ denotes the depth of root point *i*; $deep_{min}$ and $deep_{max}$ denote the minimum and maximum root point depths of the current root branch (shown in Appendix A: Figure A1); r_{max} and r_{min} denote the maximum and minimum x-y plane distances of the current root branch. The distribution of simulated root point cloud data obtained from circular and grid survey line sampling is shown in Figure 2b,c.

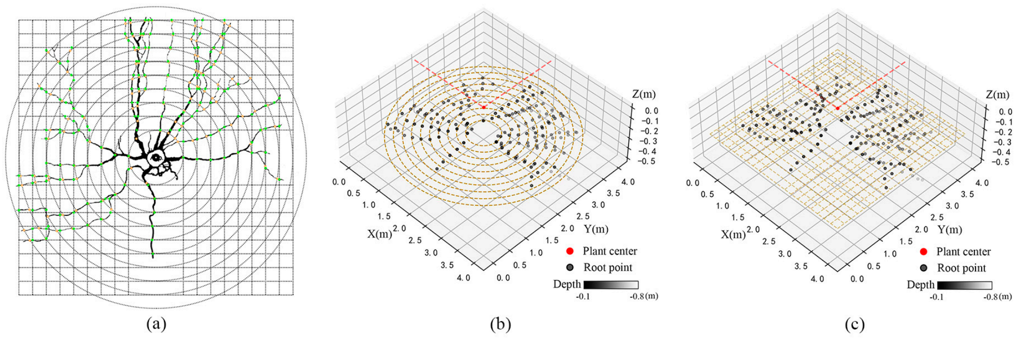

Figure 2. (**a**) Simulation data acquisition. (**b**) Simulation root point cloud data distribution under circular survey line. (**c**) Simulation root point cloud data distribution under grid survey line.

2.1.3. GPR Data Processing

The field-acquired GPR images require preprocessing to improve the signal-to-noise ratio, which contributes to the accuracy of root point identification. In this study, GPR images were preprocessed using matGPR [31]. The preprocessing steps contain the first break correction, background noise removal, filter denoising, and image gain. This aims to correct the vertical and horizontal scales on the GPR images, suppress the banding noise, remove low- and high-frequency noises, and compensate for GPR energy attenuation, respectively [32]. The preprocessed B-scan images reduce the effect of background noise and highlight the hyperbola features of roots.

Li et al. introduced a keypoint detection branch based on YOLOv4 (You Only Look Once v4) to implement a model YOLOv4-hyperbola for identifying and locating roots in B-scan images [33]. The YOLOv4-hyperbola method introduces a hyperbola landmark regression head to directly localize hyperbolic vertices. The output dimensions are expanded to 16, incorporating the detection of five key points. Inspired by facial landmark detection approaches, this method employs the vertex to represent root position, with left/right midpoints assisting vertex localization and left/right tail points characterizing the hyperbola's aperture shape. Wing loss is adopted to enhance sensitivity to minor errors, while a weighted combination of YOLOv4's original loss and key point regression loss ensures balanced optimization. By integrating geometric feature constraints, YOLOv4-hyperbola significantly improves root positioning accuracy while preserving the efficient detection capabilities inherent to YOLOv4. However, the presence of irregular hyperbolas [34], overlapping hyperbolas [35], and potential noise interference [36] may adversely affect root target recognition. The YOLOv4-hyperbola method identifies root points based on standard hyperbolic features, which could lead to missed detections in non-ideal scenarios.

The wave velocity of electromagnetic wave propagation in the soil medium in the experimental area is determined from the reflected signal of the metal plate and then used to estimate the root point depth. The coordinates of root point positions extracted based on YOLOv4-hyperbola were then converted to the actual measured coordinates of the root system in the measurement site, thus obtaining the root point cloud data of single shrubs detected by GPR in the field.

2.2. Root Point Clustering and Connection (CC Method)

A clustering–connection (CC) method framework for the reconstruction of RSA is proposed in this study (shown in Figure 3). The method mainly consists of two parts: clustering and connection. Firstly, the root points belonging to the same root branch were clustered into one group based on the angular difference in each root branch using HDBSCAN. Secondly, the root points belonging to the same root branch were linked based on the continuity of root growth. The specific method flows as follows:

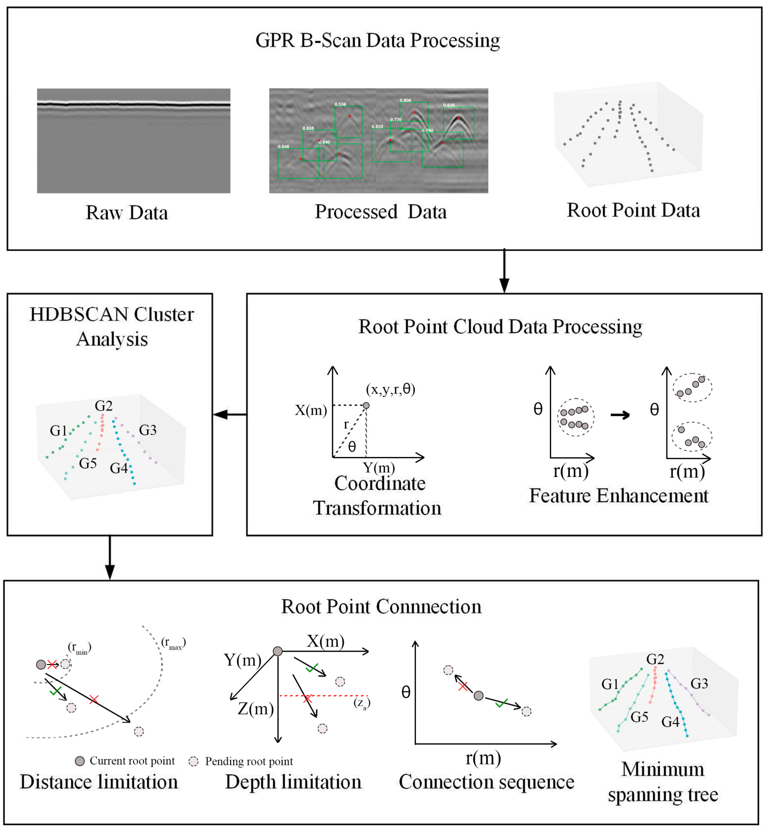

Figure 3. Conceptual diagram of the CC method framework process.

2.2.1. Coordinate Transformation and Angular Feature Enhancement

The angle between the root point and the plant center in the x-y plane is defined as the root point angle (shown in Figure 4a), which is a key attribute for extracting the root points belonging to a root branch from the complex root point cloud data. Luo et al. demonstrated that clustering based on intrinsic root attributes enables effective grouping [28]. In this study, we conduct clustering by analyzing the global distribution of root points, with the root point angle attribute (θ) serving as the central criterion. Therefore, the Cartesian coordinate system (x-y) of the root point cloud data is transformed into the characteristic coordinate system (r-θ), in which the range of the root point angle is 0–2π. The transformation formulae are not the same for the different line arrangements, in which the transformation formulae for the circular line arrangement are shown below:

$$x_i = r_{ci} \times cos\left(\frac{l_i}{r_{ci}}\right), \tag{3}$$

$$y_i = r_{ci} \times sin\left(\frac{l_i}{r_{ci}}\right), \tag{4}$$

$$\theta_i = \frac{l_i}{r_{ci}}, \tag{5}$$

where the actual site coordinate position of the root point under the circular survey line arrangement is (x_i, y_i). r_{ci} denotes the radius length corresponding to the radius of the root point subordinate to the survey line segment numbered ci, θ_i denotes the root point angle, and l_i denotes the transverse coordinate position of the root point on the B-scan image.

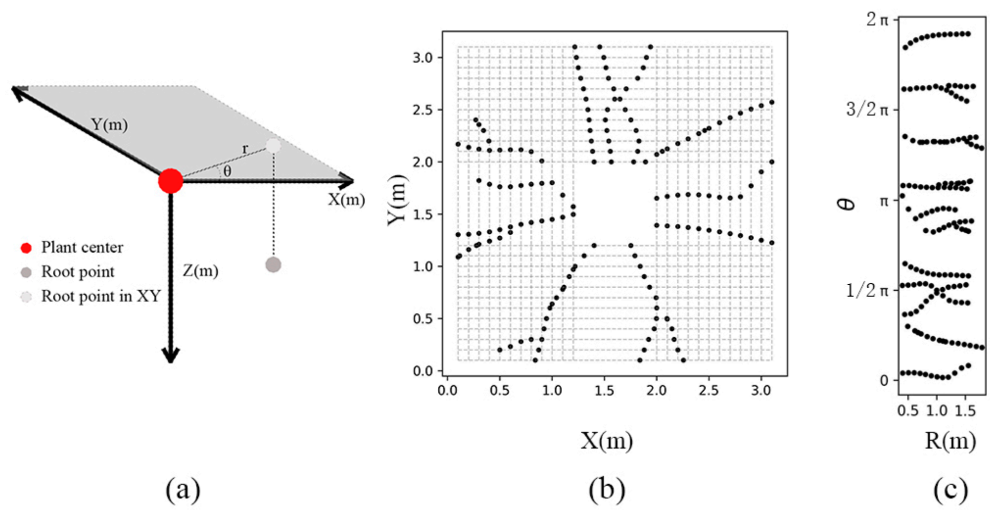

Figure 4. (**a**) Schematic diagram of coordinate space transformation, θ denotes the root point angle, and r denotes the distance from the center of the plant in the x-y plane. (**b**) Root point planar coordinate system before transformation. (**c**) Root point characteristic coordinate system after transformation, which is expressed as example data.

The transformation of the grid line arrangement differs from circular, and the transformation formula is shown below:

$$r_i = \sqrt{(x_i - x_c)^2 + (y_i - y_c)^2}, \tag{6}$$

$$\theta_i = \begin{cases} arccos\left(\frac{x_i - x_c}{r_i}\right) & y_i - y_c \geq 0 \\ arccos\left(\frac{-x_i - x_c}{r_i}\right) + \pi & y_i - y_c < 0 \end{cases} \tag{7}$$

where (r_i, θ_i) are the r and θ attributes of root point i after conversion to the characteristic coordinate system, respectively. (x_i, y_i) are the planar position coordinates of root point i, and (x_c, y_c) is the position of the plant center. Compared with the original root point cloud data, the converted root point cloud data enlarges the distance between the root points near the plant center, while reducing the distance between the root points away from the plant center. Root points are mainly converged by their angular information so that the root points belonging to the same branch are more clustered (shown in Figure 4b,c).

To increase the distance between different root branches while simultaneously reducing the distance between root points within the same branch, the angle θ of each root point after coordinate transformation is enlarged by a factor of four.

After the coordinate space transformation and angular feature enhancement, the root point cloud data with prominent angular attributes is obtained. After the above data processing: each root point has the following spatial attributes, which can be expressed as p(r, θ, x, y, z).

2.2.2. HDBSCAN Cluster Analysis

In this study, the HDBSCAN (Hierarchical Density-Based Spatial Clustering of Applications with Noise) method was used to perform clustering analysis on the root point cloud data. HDBSCAN mainly integrates the ideas of density clustering and hierarchical clustering and can deal with different densities of the data distribution and identify the cluster structure of any shape in the data. Moreover, the method does not need to prespecify the number of clusters in the process of use. The parameter adjustment is simple and intuitive, and it is robust to noise and outliers, which is suitable for more complex data patterns [37]. The root point cloud data are non-convex data with a different density space, and therefore, are suitable for cluster analysis using HDBSCAN. The core of HDBSCAN is the use of mutual reachability distance to measure the distance between points, which is calculated as follows:

$$d_{mreach-k}(a,b) = max\{core_k(a), core_k(b), d(a,b)\}, \quad (8)$$

where $d_{mreach\text{-}k}(a,b)$ is the mutual reachability distance between point a and point b. $core_k(x)$ is defined as the core distance of x, which is the nearest neighbor distance of a point to its k point, so $core_k(a)$ is the core distance of point a, $core_k(b)$ is the core distance of point b, and $d(a,b)$ is the euclidean distance between point a and point b. The mutual reachability distance can separate the low-density area from the high-density area of the root point cloud data, thus achieving the effect of identifying different density spaces. Based on the data processing results in Section 2.2.1, we use the r and θ attributes of the root points to perform cluster analysis and calculate the mutual reachability distance between different root points.

The minimum spanning tree is constructed by taking the mutual reachability distance between root points as the edge weights (shown in Figure 5a), and the cluster hierarchy is obtained by incrementally ordering the edge weights (shown in Figure 5b). The cluster hierarchy is compressed and partitioned according to the condition of minimum clusters (m), root clusters smaller than the minimum number of clusters (noisy root points) are screened out (shown in Figure 5c), and the potential root branch classification is obtained by excluding noisy root points. The stability of clusters can be evaluated by the stability index $S_{cluster}$, which is calculated as follows:

$$S_{cluster} = \sum_{p \in cluster} (\lambda_p - \lambda_{birth}), \quad (9)$$

where $S_{cluster}$ denotes the stability index, λ_p denotes the reciprocal of the mutual reachability distance when the root point p is separated from the cluster, and λ_{birth} denotes the reciprocal of the mutual reachability distance when the new cluster is split. The stability metric is mainly a judgment metric to determine whether two root point clusters can be merged into one root point cluster. If the sum of the stability of the two root point clusters is less than the stability before splitting, the two clusters are merged.

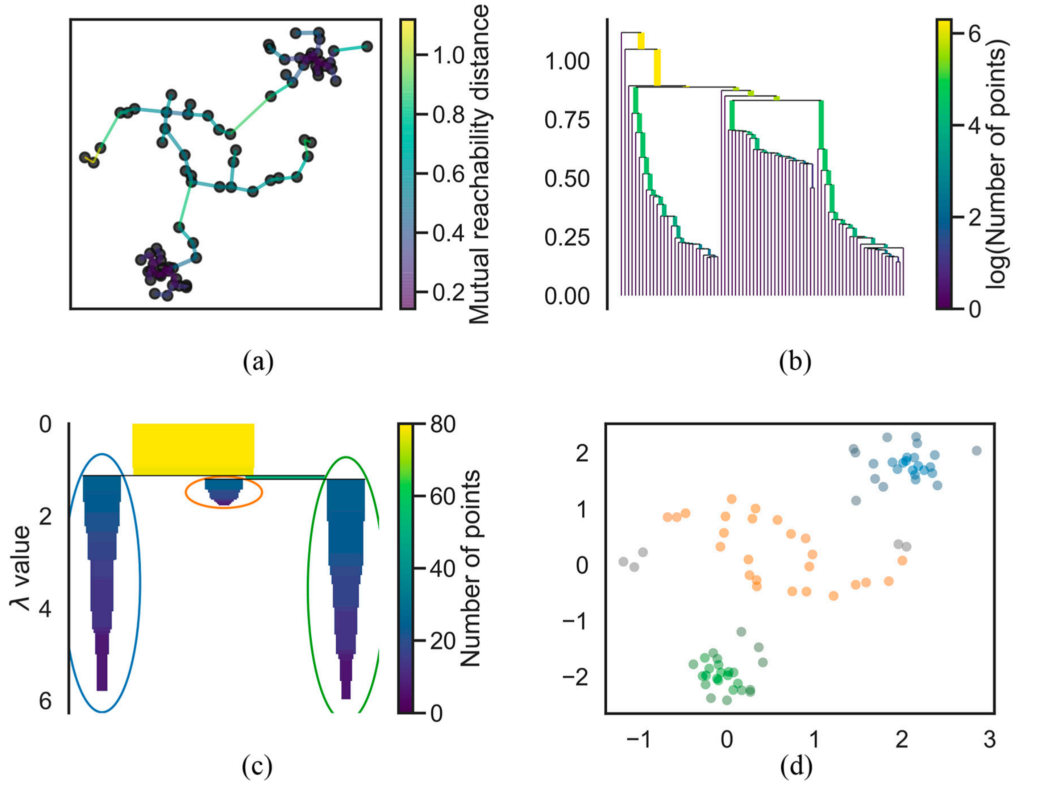

Figure 5. HDBSCAN schematic. (**a**) Minimum spanning tree based on mutual reachability distance, (**b**) build the cluster hierarchy, (**c**) condense the cluster tree and extract the clusters, (**d**) final clustering results, different colours mean different clusters.

The HDBSCAN algorithm in this study only requires the setting of the basic parameter min_cluster_size, which represents the minimum cluster size, i.e., the minimum number of root points in the root branch obtained by clustering. This parameter depends on the line interval and the size of the root system during the actual measurement. The smaller the line spacing is, the denser the root points are. The more root points are included in the root point cloud data, the larger the value is. Based on previous research and empirical testing of HDBSCAN on root point cloud data [38], in order to achieve the most reasonable clustering results and the least number of noisy root points, the min_cluster_size parameter in this study can be set to 2.

2.2.3. Root Point Connection

The reconstruction of a root system topology needs to take into account the spatial continuity of root branches. Based on the root system parameters traditionally utilized in root architecture reconstruction, three critical factors include inter-root distance [27], root depth hierarchy [26], and connectivity sequence [23] are prioritized. Therefore, we set up three root point connection rules to determine whether the two root points can be connected. (1) Distance limitation: If the distance between the two root points is too large, it means that the spatial connection between the two root points is weak, so they will not be connected. Similar root points on the same survey line with similar values of r attribute, but the θ attribute may be quite different, and thus there may be other root branches, which will not be connected. Specifically, the distance between root points needs to be greater than 1/4 (r_{min}) and less than 2 (r_{max}) times the survey line interval, so the distance limitation is expressed as ($r_{min} < r_i - r_j < r_{max}$). (2) Depth limitation: If the depth difference between root points is greater than the set depth threshold (z_a), it can be considered that the two root points belong to two root branches and will not be connected. Specifically, the depth limitation is expressed as ($|z_i - z_j| < z_a$). (3) Connection sequence: the connection of root points strictly follows the principle of from near to far, i.e., expanding the connection outwards with the plant as the center ($r_i < r_j$).

Several clusters of root points can be obtained by clustering analysis, where root points within the same cluster are relatively clustered in terms of the θ attribute, while root points between different clusters are relatively far away from each other. Therefore, we assume that each cluster of root points obtained by clustering belongs to the same root branch, and a root branch can be obtained by connecting the root points within the cluster. Plants tend to take the smallest resources to obtain more energy, so a minimum spanning tree (MST) is used to connect all the root points that meet the connection rules within the root point clusters to minimize the connection cost. The Euclidean distance is used as the weight between root points, which is calculated as follows:

$$\mathrm{d_{ij}} = \sqrt{(\mathrm{x_i} - \mathrm{x_j})^2 + \left(\mathrm{y_i} - \mathrm{y_j}\right)^2 + (\mathrm{z_i} - \mathrm{z_j})^2}, \quad (10)$$

where $\mathrm{d_{ij}}$ is the weight reference of the two root points to construct the minimum spanning tree, in which ($\mathrm{x_i}$, $\mathrm{y_i}$, $\mathrm{z_i}$) and ($\mathrm{x_j}$, $\mathrm{y_j}$, $\mathrm{z_j}$) are the position coordinates of root point i and root point j, respectively. When constructing the adjacency matrix, the two root points must meet the three rules mentioned above. Otherwise, they are excluded from the calculation. The adjacency matrix is constructed based on the weights d. The Prim algorithm is used to obtain the result of the minimum spanning tree for the constructed adjacency matrix.

The root system topology was obtained after two steps of root point clustering and root point connection. In order to reconstruct the RSA more graphically, the root system topology was smoothed by spline curves with reference to the method proposed by Wu et al. [23], and then the RSA of the plant was reconstructed in AutoCAD 2020 (Autodesk Inc., San Francisco, CA, USA).

2.3. Method Evaluation

The accuracy of the method proposed in this study is quantitatively evaluated by the root point connection accuracy rate, which is obtained by calculating the ratio of the number of correctly connected root points to the number of all connected root points, and the calculation formula is shown below:

$$\mathrm{R} = \frac{\mathrm{Num_c}}{\mathrm{Num_s}} \times 100\%, \quad (11)$$

where R is the connection accuracy rate, $\mathrm{Num_c}$ is the number of root points connected correctly, and $\mathrm{Num_s}$ is the total number of root points in the connection.

Since the root point cloud data in this paper only includes root point coordinates, the effectiveness of the CC method in this paper is quantitatively evaluated by root length. The total root length of the coarse root system is calculated by summing the Euclidean distances between all connected root points in the CC method. The length of the root segment between two connected root points, root points i and root points j, which is written as L_{ln}; its calculation formula is as follows:

$$L_{ln} = \sqrt{(\mathrm{x_i} - \mathrm{x_j})^2 + \left(\mathrm{y_i} - \mathrm{y_j}\right)^2 + (\mathrm{z_i} - \mathrm{z_j})^2}, \tag{12}$$

where L_{ln} denotes the Euclidean distance of the two root points, in which ($\mathrm{x_i}$, $\mathrm{y_i}$, $\mathrm{z_i}$) and ($\mathrm{x_j}$, $\mathrm{y_j}$, $\mathrm{z_j}$) are the positional coordinates of root point i and root point j, respectively. The total root length of the coarse root system is determined by summing the distances between all root points and is calculated using the following formula:

$$L = \sum_{n=1}^{m} L_{ln}, \tag{13}$$

where L denotes the total root length of the coarse root system, L_{ln} denotes the Euclidean distance of the two root points, and m denotes the total number of root segments reconstructed using the CC method. The total root length of the correctly connected coarse root system is calculated using the same method. The effectiveness of the reconstruction method was measured by the rate of root length deviation (RootLD), where the formula for the rate of root length deviation is shown below:

$$\mathrm{RootLD} = \frac{|\mathrm{L_{rec}} - \mathrm{L_{sim}}|}{\mathrm{L_{sim}}} \times 100\%, \tag{14}$$

where RootLD is the root length deviation rate, and $\mathrm{L_{rec}}$ with $\mathrm{L_{sim}}$ are the total root length of the reconstructed coarse root system and the total root length of the correctly connected root system, respectively. The smaller the value of RootLD indicates that the effectiveness of the reconstructed RSA is better, and the smaller the difference with the correct root length.

3. Results

3.1. RSA Reconstruction of the Simulated Data

The clustering results of the simulated root system data are shown in Figure 6b,d. Different colors in the figure represent different clusters of root points obtained by clustering. The parameter (min_cluster_size) is set to 2 in both scenarios. The results show that the root points belonging to different root branches are clustered into one group. In the case of circular survey line measurement, root points are clustered into 10 classes, with four root points identified as noise. In contrast, with grid survey line measurement, root points are clustered into 12 classes, and seven root points are identified as noise. Most of the clustering results are the same under both survey line layouts, and the same clusters of root points are obtained, such as G0, G1, G2, G3, G5, G6, G7, and G8 in Figure 6b, which correspond to G0, G1, G2, G3, G6, G7, G8, and G9 in Figure 6d. For roots with no secondary root bifurcation, such as G0, G6, and G8 in Figure 6b and G0, G7, and G9 in Figure 6d, the clustering results under both survey line layouts are completely consistent. In these cases, the angular consistency of the roots within the same category is stronger, resulting in the best clustering effect. However, the two scenarios also show different clustering results, which are mainly reflected in the clustering results of G4 and G9 under the circular survey line (shown in Figure 6b), which are divided into two categories under the grid survey line and become G4, G5, and G10, G11 (shown in Figure 6d).

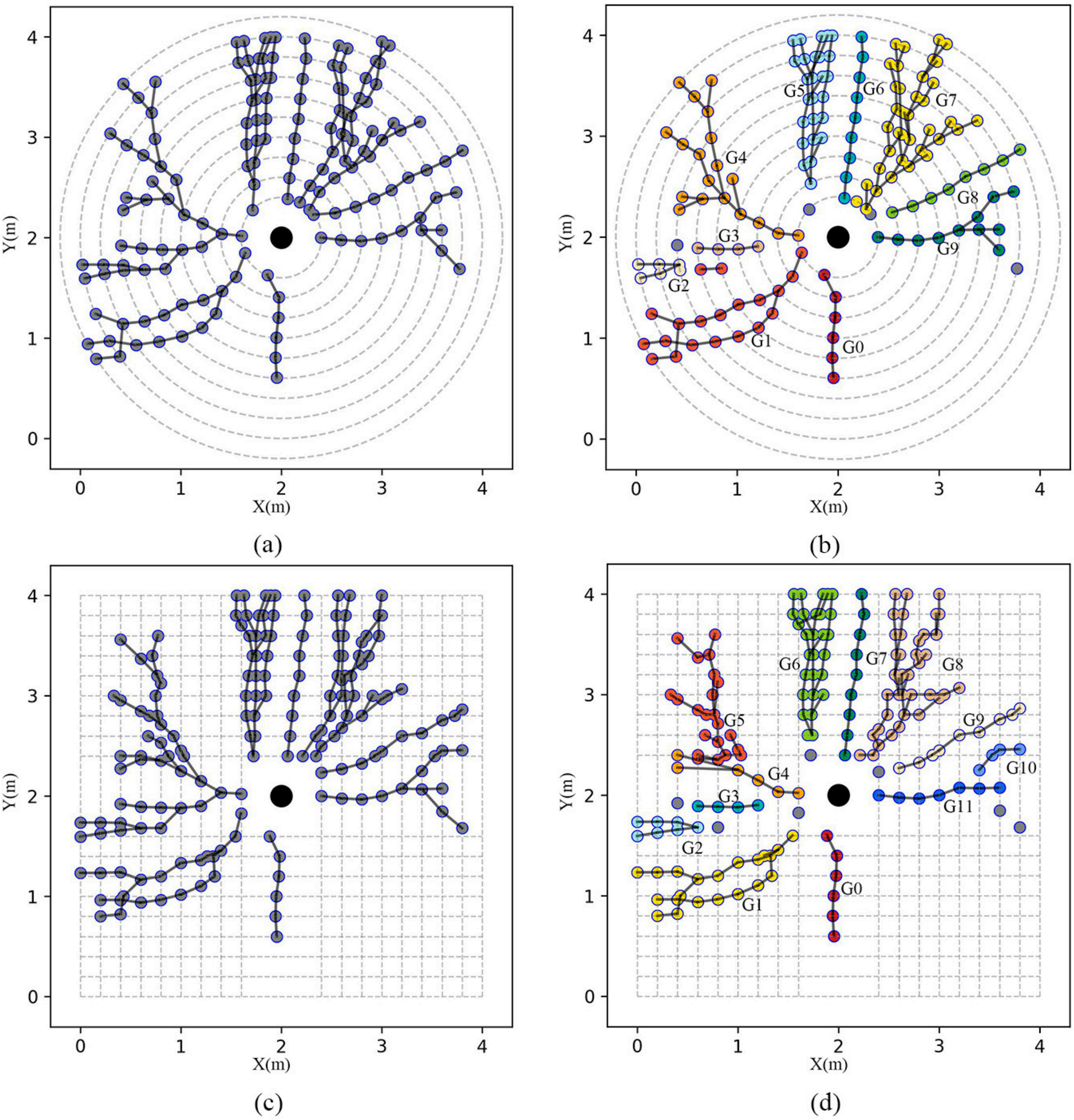

Figure 6. Root connection results. (**a**,**c**) are the correct root connections for the circular and grid survey line layouts, and (**b**,**d**) are the root connection results for the CC method.

The values of r_{min} and r_{max} were set to 0.05 m and 0.4 m, respectively, as the survey line interval was 0.2 m. Through several depth threshold attempts, the accuracy of the RSA connection was the highest under the two survey lines when the depth threshold z_a value was taken as 0.04 m, which was 93.38% under the circular survey line and 88.17% under the grid survey line. The root point connection results are shown in Figure 6. Figure 6a,c represent the correct topological connection relationships. Figure 6b,d represent the topological relationships obtained by the CC method, where the numbering of the root clusters follows the results of the root point clustering. The connection results present the following features: (1) If there is no secondary branching of a root in a certain direction, such as G0, G6, G8 in Figure 6b, and G0, G7, G9 in Figure 6d, the root can be reconstructed accurately. (2) If the branching angle of the secondary root is small relative to the superior root, G1, G5 in Figure 6b, and G1, G6 in Figure 6d, the root point on that root also has a reliable connection accuracy. (3) If the branching angle of the secondary root is large relative to the superior root, such as G4, G7 in Figure 6b and G5, G8 in Figure 6d, it will lead to an increased probability of root point connection error and an unrealistic root point connection. (4) Since a small number of roots are identified as noise points in the clustering step, these root points do not participate in the connection step, which results in a root connection error, such as G3, G9 in Figure 6b and G2, G3, G11 in Figure 6d.

Figure 7 shows the 3D RSA reconstruction results of the simulated coarse root system for the circular (Figure 7a) and grid (Figure 7b) survey line layouts. Based on this, we calculated the RootLD for the two scenarios separately. The RootLD for the circular line was 3.23%, with the total root length reconstructed by the CC method measuring 29.67 m, and the total root length of the correctly connected roots being 30.66 m. For the grid line, the RootLD was 9.17%, with the total root length reconstructed by the CC method at 28.04 m, and the total root length of the correctly connected roots measuring 30.87 m. This demonstrates the effectiveness of the CC method in reconstructing the 3D RSA under both survey line layouts.

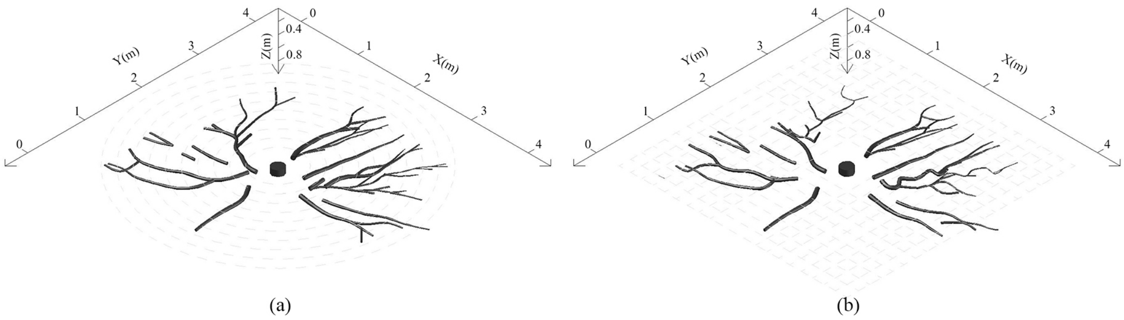

Figure 7. Reconstruction results of 3D architecture of plant coarse root system from simulated data (**a**) circular survey line layout (**b**) grid survey line layout.

3.2. RSA Reconstruction of the Field Measured Data

Figure 8 shows the root morphology map of the field excavation (shown in Figure 8a) and the distribution of the coarse root point cloud data detected and identified using GPR for different survey line measurement methods (shown in Figure 8b,c). The root point distributions acquired from the two survey line layouts exhibit distinct differences. Compared to the grid survey line layout, the circular survey line layout is more effective in detecting the direction of the root system, as roots are more continuously distributed.

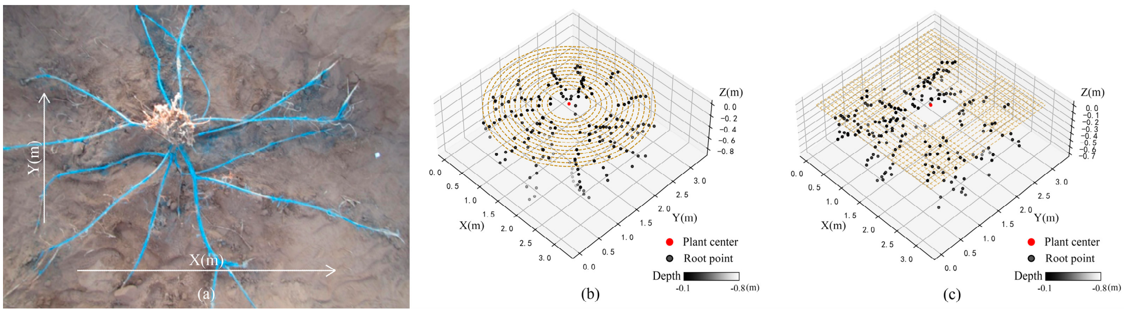

Figure 8. (**a**) Field measured root system, field photo. (**b**) Circular survey line root point distribution. (**c**) Grid survey line root point distribution.

To quantitatively assess the effectiveness of the reconstructed RSA connection, the root point cloud data obtained from the two survey line layouts were manually connected, serving as a reference for the correct root point connection in the field data (shown in Figure 9a,c). The parameters of the CC method in the field data are as follows: the

HDBSCAN clustering parameter in the root point clustering is still defaulted to 2, r_{min} and r_{max} in the root point connection are set as 0.025 m and 0.2 m, respectively. The only depth threshold in the CC method that required multiple adjustments was selected as 0.06 m for both scenarios. Finally, we obtained the topological connection of the RSA (shown in Figure 9b,d). In the clustering step, the black root points represent identified noise and are excluded from subsequent connection processes. For the circular survey line, the root point cloud data were divided into 18 groups. As shown in Figure 9b, groups G0, G2, G5, G6, G7, G8, G12, and G14 were successfully extracted due to their distinct angular distribution characteristics of root points. However, groups G3, G4, G9, G10, G13, G15, and G16 despite being detected were fragmented into 2–3 subgroups owing to missing intermediate root points and uneven spatial distribution. In the grid survey line layout, the root point cloud data were partitioned into 17 groups. In Figure 9d, groups G0, G1, G4, G9, and G11 exhibited robust extraction results. Similarly to the circular case, groups G6, G7, G15, and G16 in the grid line were split into two subgroups due to irregular point dispersion. Notably, groups G8 and G14 in the grid survey line layout (unlike the circular scenario) lacked identifiable root extension direction features and were aggregated into a single category, which may compromise the accuracy of subsequent connection steps.

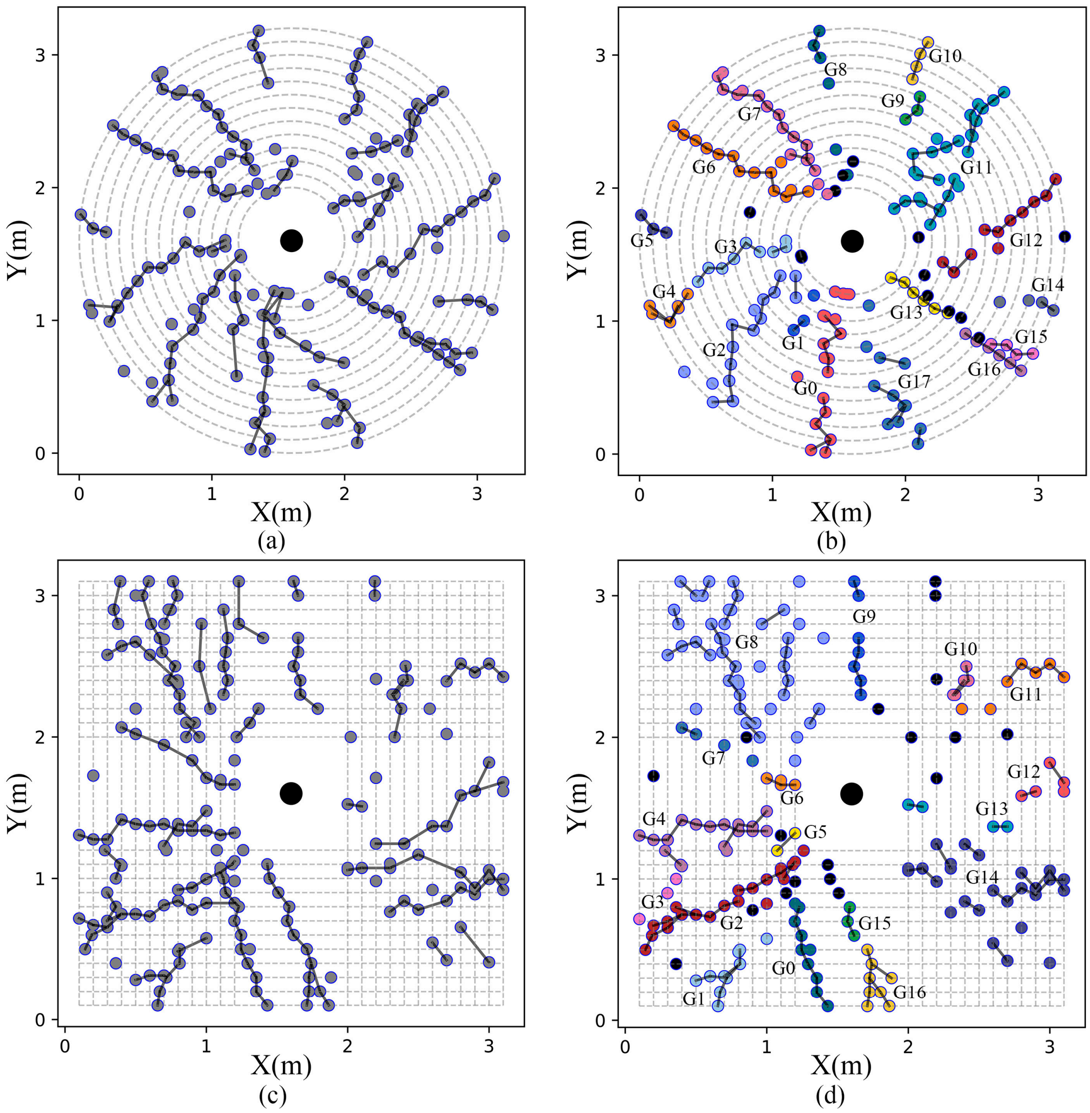

Figure 9. Field data manually connected results with (**a**) circular and (**c**) grid survey line layouts, CC method connected results with (**b**) circular and (**d**) grid survey line layouts.

Compared with the correct root point connections manually connected, the connection accuracy reached 83.77% in the circular survey line layout and 72.25% in the grid survey line layout. In the validity evaluation, the total root length of the correct root system was 17.67 m and 19.7 m for the circular and grid line scenarios, respectively, while the root length deviation (RootLD) was 22.3% and 32.34% for the two survey line scenarios, respectively.

The 3D RSA reconstruction results of the measured root system under different survey line layouts after processing by the CC method and 3D visualization are shown in Figure 10. As observed in the orange boxed area, the continuity of root branches is better under the circular survey line layout, whereas the grid survey line layout results in more discontinuous root segments. From the green boxed area, it can be seen that the grid survey line layout collects more root point data than the circular layout, and the grid reconstruction performs better when there is sufficient local root point information. In the blue boxed area, it is evident that the blue-labeled points exhibit similar structure. However, in the circular survey line arrangement, the identified root point locations may have slight deviations along the survey line due to errors in the arrangement and measurement process.

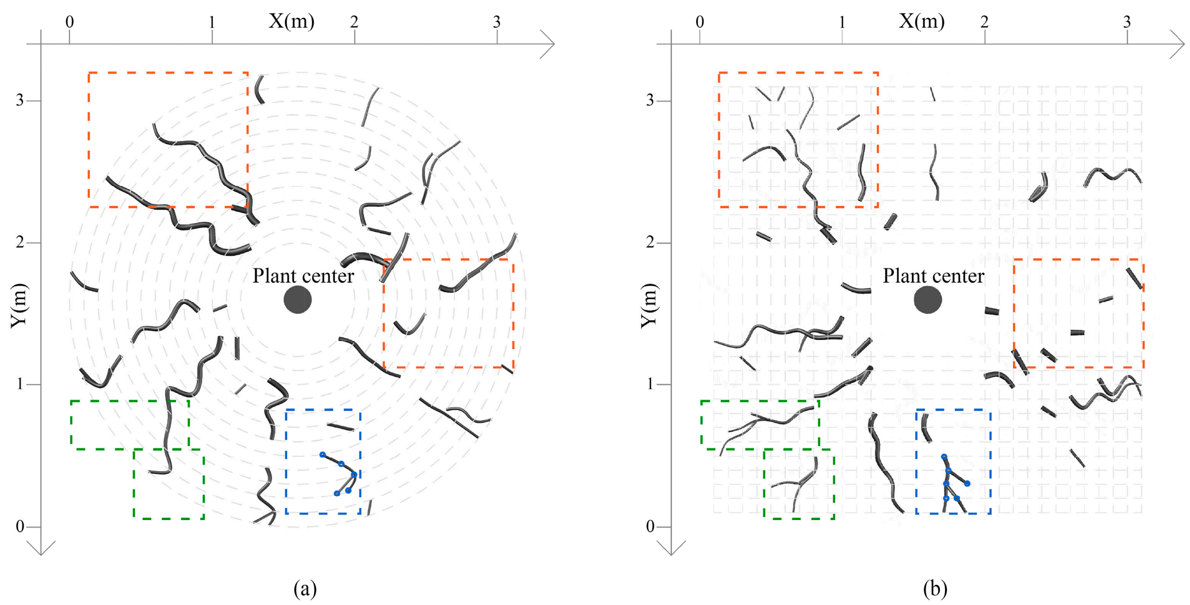

Figure 10. Reconstruction results of the 3D architecture of the shrub coarse root system from field data (**a**) circular survey line layout and (**b**) grid survey line layout.

4. Discussion

4.1. Advantages of the Method

The CC method accommodates multiple arrangements by adopting a strategy that prioritizes a global perspective, then focuses on local details, and finally integrates local information back into the global context. From a global perspective, the spatial distribution pattern of root points shows the aggregation and dispersion characteristics of the root system. These characteristics are closely related to the RSA. Therefore, our approach begins with a global perspective. The root orientation information is derived from the spatial distribution of root points and is used to cluster the root points belonging to the same branch into the same group by HDBSCAN. Then, we connect the root points of each root branch separately to finally reconstruct the RSA of the whole root system. This helps to capture the morphological features and topological relationships of the root system and accurately locate each root branch, thus improving the accuracy of the root point connections. It makes the method extremely easy to use and allows for intuitive observation of the 3D topology of the root system.

To verify that the CC method performs well on different survey line layout, the method proposed by Wu et al. [23] is selected for the circular survey line arrangement, while the method proposed by Fan et al. [27] is chosen for the grid survey line arrangement for comparison. Table 1 shows the results of the comparison between the CC method and the existing research methods. It can be seen that, compared with the previous methods, the root point connection accuracy (R) obtained by the CC method has been improved for both the simulated data and the measured data under the measurements of the circular m grid survey line set. Wu's method uses different search window settings for connection, which can result in incorrect root point connections in cases of complex, overlapping root branches. In contrast, the CC method effectively addresses this issue by applying a minimum spanning tree and rule-based restrictions, leading to an improved R value. Fan's method faces challenges in setting the deviation angle threshold. If the threshold is too small, some root branches cannot be connected because their deviation angles exceed the set limit. Conversely, if the threshold is too large, incorrect connections may occur. This contributes to a key issue highlighted by Fan, in order to ensure the continuity of the reconstructed root system, the root point utilization was relatively low, which resulted in a low R value. The CC method, by searching for as many valid connections as possible in the detected root point cloud data, achieves a higher relative R value. The CC method mainly consists of inputting the root point cloud data, the coordinate of plant center coordinates, survey line spacing, and determining the min_cluster_size and depth thresholds and then, a 3D topological schematic of the root system can be obtained in Python 3.9. The time required to complete the entire method process is approximately 12 s.

Table 1. Comparison of R value of CC method with other methods and survey line layout forms.

	Simulated (R)	Measured (R)	Survey Line Form
CC method	93.38%	83.77%	Circular
Wu	89.4%	79.22%	Circular
CC method	88.17%	72.25%	Grid
Fan	81.07%	69.36%	Grid

Secondly, the CC method uses coordinate transformations to further emphasize and utilize the root orientation information. The root orientation is crucial for determining the effectiveness of RSA reconstruction based on GPR-identified root point cloud data [28]. The spatial coordinate system (x, y, z) was transformed into a feature space system (r, θ, z) with the shrub center as the origin, further highlighting and utilizing root orientation information. This transformation effectively distinguishes the extension direction of different roots during analysis, enhancing the method's ability to identify roots growing in the same direction and making the root orientation more comprehensively utilized. A comparison of the HDBSCAN clustering results before and after the transformation is shown in Figure 11. It can be seen that the clustering results after coordinate transformation enhance the rationality of the clustering and improve the effectiveness of RSA reconstruction (Figure 11b). The coordinate conversion effectively resolved two problems. On the one hand, root points on different root branches that are closely connected are easily clustered into one class (class G1 in Figure 11a). On the other hand, root points on the same root branch are clustered into different types due to the difference in the density of root point distributions (G5, G6, G7, G8, and G9 in Figure 11a).

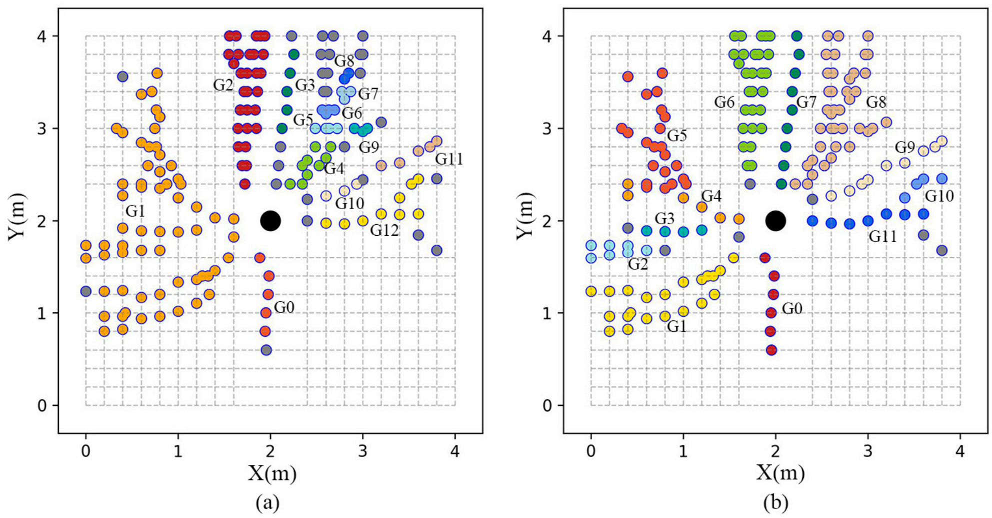

Figure 11. (**a**) Clustering results before the coordinate transformation. (**b**) Clustering results after the coordinate transformation.

Unlike most previous studies that rely on a single survey line arrangement [23,26–28]. The CC method adapts to various scenarios, as it is not restricted to a specific survey line arrangement. The distribution of root points differs between those collected using circular and grid survey lines (shown in Figures 2 and 8). This difference becomes even more pronounced in the measured data. However, the CC method is designed to handle these data variations and effectively reconstruct the RSA. By simply inputting the root point cloud data and the plant center coordinates, the topological structure of the root system can be obtained. Therefore, the concept of overall–local–overall enables the CC method to bypass the limitations of specific survey line arrangements, expanding its applicability to a broader range of scenarios.

4.2. Analysis of RSA Reconstruction Under Different Scenarios

Comparing the reconstruction results of the simulated and measured data, it can be found that the continuity of the RSA reconstructed from the measured data is poor under the two survey line scenarios, and this led to a lower reconstruction accuracy (Table 2). There are two main reasons for this: Firstly, due to the influence of surface micro-topography, the GPR antenna may deviate from the pre-set survey line position during manual dragging close to the ground. Combined with uncertainties in post-data processing, the final decoded root point positions may not precisely match their actual locations. Secondly, it is related to the actual detection rate of GPR on the root system in the field environment. Due to the complexity of the soil medium in the field, GPR may have missed detection in root detection. This results in a discontinuous spatial distribution of root points on certain root branches in the measured data. Simulated data can avoid the above issues, resulting in better reconstruction results in both scenarios compared to measured data.

Table 2. Reconstruction results for simulated and measured data.

	Survey Line Layout	Total Number of Root Points	R	RootLD
Simulated data	Circular	151	93.38%	3.23%
	grid	169	88.17%	9.17%
Measured data	Circular	185	83.77%	22.3%
	grid	200	72.25%	32.34%

Comparing the reconstruction results under the two arrangements of the survey line, it can be found that the reconstructed RSA under the grid survey line arrangement is much more discrete than that under the circular survey line arrangement (shown in Figure 10). This is mainly because circular survey lines can maximally ensure that the measurement direction of GPR is perpendicular to the extension direction of the subsurface root system. This is so that the optimal reflection signals can be obtained and the bias and missed rate of the root location can be reduced [34,39,40]. The grid survey line has two definite measurement directions, although, it can make up for the missing measurement of root points caused by a single direction. The root reflection signals are still too weak or cannot be decoded due to the small angle between the roots and the measurement direction of the GPR antenna. Therefore, the continuity of the root distribution in the root point cloud data obtained from the circular survey line arrangement is better, and the reconstructed root system is more smooth and complete. If the field measurement conditions permit, it is recommended that the circular survey line arrangement should be preferred.

4.3. Sensitivity Analysis of Parameters

The sensitivity analysis focuses on two critical parameters in the CC method, The min_cluster_size parameter serves as a density threshold that governs the aggregation of root point cloud data with similar attributes. This parameter directly determines the granularity of initial root segment identification, thereby fundamentally influencing the accuracy of the subsequent connection step.

To quantitatively evaluate parameter sensitivity, Figure 12 presents clustering results from simulated circular survey line data under varying min_cluster_size configurations. The experimental data reveal an inverse relationship between parameter magnitude and classification outcomes. It shows that as min_cluster_size increases, the number of classifications decreases, while the number of noise root points increases. Cui et al. [38] applied the HDBSCAN method to perform quadrat-scale cluster analysis of root point clouds data, achieving individual shrub segmentation, while systematically investigating the parameter min_cluster_size. Different soil conditions (e.g., sandy vs. clayey soils) remain a variable factor in our research, while their impact lies in the initial B-scan image acquisition rather than the core methodological steps addressed here. Therefore, soil conditions have limited influence on the selection of optimal parameters in our method. Building on these methodological foundations, we empirically determined min_cluster_size = 2 as the optimal value for both simulated and field datasets in this study.

The depth threshold (z_a) was systematically evaluated by measuring root point accuracy (R) across both circular and grid survey line layout in simulated data. As quantified in Table 3, the optimal z_a value of 0.04 m consistently maximized R in both scenarios. Setting z_a too small results in larger errors when the depth between connectable root points exceeds the threshold. Conversely, setting z_a too large has minimal impact on root point connection selection, and the root point accuracy remains unchanged.

Table 3. The R values for different line arrangements at various z_a values in the simulated data.

z_a	0.02	0.03	0.04	0.05	0.06	0.07
Circular (sim)	83.44%	92.72%	93.38%	92.72%	92.05%	92.05%
Grid (sim)	82.25%	86.39%	88.17%	88.17%	87.57%	87.57%

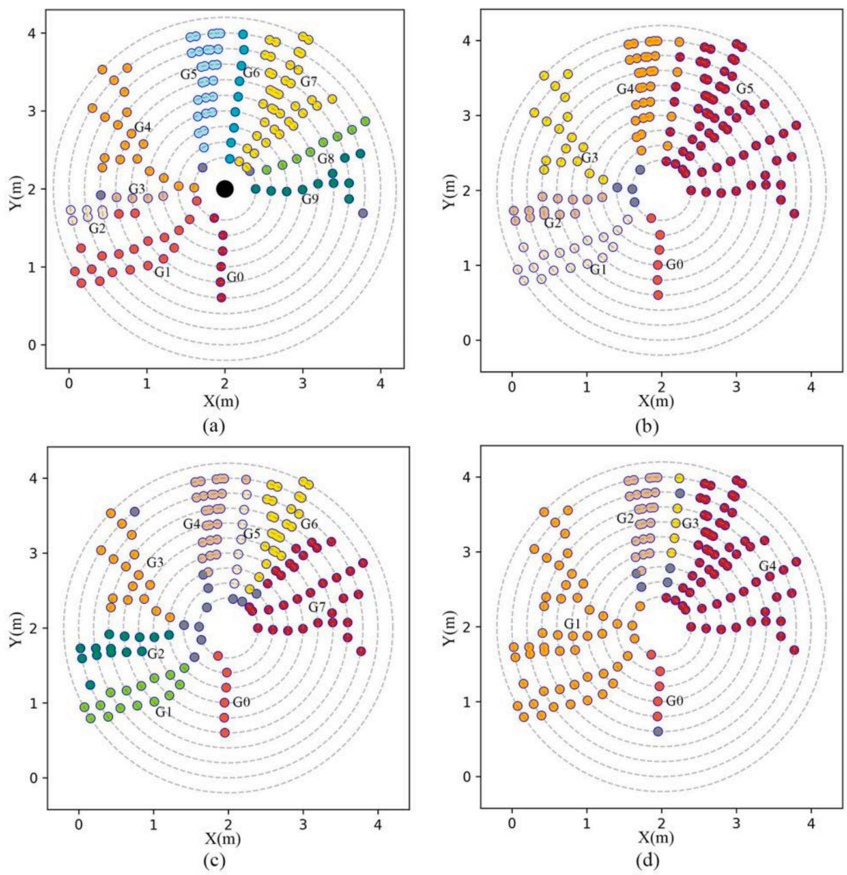

Figure 12. Clustering results with different parameters setting. (**a**–**d**): 2–5.

We also analyzed the number of root points and their cumulative percentages at each depth, using 0.1 m intervals, with circular survey lines in both simulated and measured data. We found that the depth threshold is typically set near the ratio of depth to the number of lines when the cumulative percentage of root points reaches 80% or more (shown in Figure 13). For example, in the simulation data, when the cumulative percentage of the root points exceeds 80%, the depth range is 0.4 m, with 10 lines, so the depth thresholds are centered around 0.04 m. This suggests a strong relationship between the depth threshold, the distribution of the shrub's root points, and the number of survey lines. When applying this to other plants, the depth distribution and number of survey lines can be prioritized to quickly determine a suitable depth threshold.

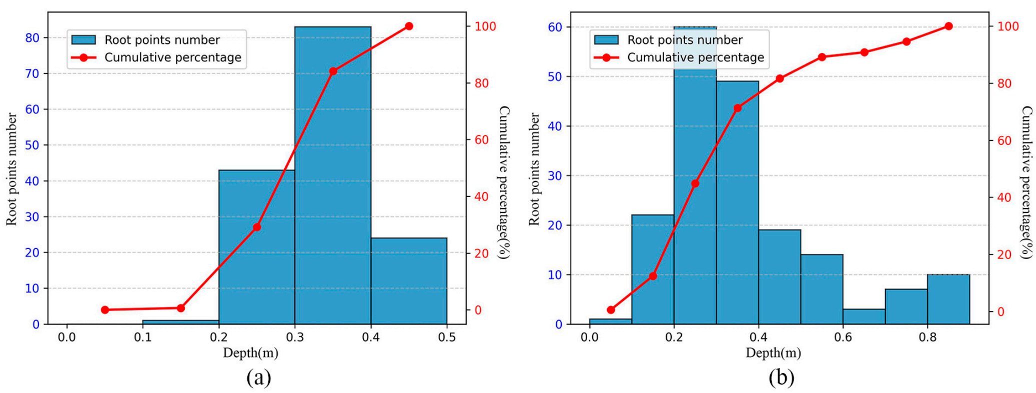

Figure 13. Distribution and cumulative percentage of root points in a circular line arrangement for simulated (**a**) and measured data (**b**).

4.4. Limitations of the Method and Future Outlook

Although the CC method performs well in terms of reconstruction results, it still has some limitations. These include GPR's technical limitations, the complex growth patterns of root systems, the inherent limitations of the HDBSCAN, and measurement errors in field experiments. Firstly, the technical limitations of GPR can impact the quality of the root point cloud data obtained. The resolution of GPR is inversely related to the antenna frequency, as higher frequencies result in lower resolution. Previous studies have shown that GPR is more effective in detecting coarse roots [41], which exhibit clear hyperbolic characteristics, while fine roots are harder to detect due to their weaker reflection of electromagnetic waves. As a result, the application of CC methods for detecting fine roots is limited, which is a challenge faced by all GPR-based algorithms for reconstructing RSA. Secondly, The complex growth patterns of the root system may affect the reconstruction effect of the CC method. Complex root growth patterns, including multi-branching, highly intertwined, and high root density, may cause the hyperbolic signals on the radar map to overlap with each other, making it more difficult to decipher the root signals, which in turn affects the reconstruction effect of the CC method. Although our method improves reconstruction accuracy by considering root growth characteristics and orientation, the connectivity and clustering of root points may still lack sufficient accuracy in highly complex root environments. Thirdly, HDBSCAN will judge some outlying root points as noise points, which leads to a certain degree of omission of valid root points. However, in terms of the reconstruction effect, this type of error accounts for a small percentage and is negligible (2.65%, 4.14%, and 7.03%, 9% in both two scenarios in simulated and measured data, respectively). Finally, field experimental conditions affect radar detection, including the soil environment and manual measurement errors. Studies have shown that ground-penetrating radar is more effective in sandy soil with good drainage and less effective in clay soil [42]. Additionally, deviations in the measurement line caused by the experimenter during field measurements can impact the accuracy of the root data obtained.

Despite the aforementioned limitations, its application potential in complex root scenarios and diverse plant species can be significantly enhanced with the continuous advancement of Ground-Penetrating Radar (GPR) equipment and image processing technologies. The specific improvement directions include the following: Firstly, there exists a trade-off between GPR resolution and detection depth, as higher antenna frequencies improve resolution but reduce penetration depth [17]. Developing a multi-frequency GPR image fusion method that effectively combines high-frequency near-surface data with low-frequency deep-layer data could substantially enhance root identification accuracy. Secondly, strengthening root feature recognition capabilities and environmental noise resistance through machine learning or deep learning techniques will significantly improve RSA reconstruction. For instance, the Yolo-v4hpd network proposed by Cui et al. [43] has demonstrated effective extraction of root diameter information from noisy field data. ParaNet, proposed by Sun et al. [44], employs multi-polarimetric radar to estimate multiple root parameters. Integrating multi-source root characteristic parameters could further enhance reconstruction robustness in complex root environments or fine root. By interpreting additional root parameters, it is possible to group root points with similar characteristics into comprehensive clusters during the clustering phase based on distinct features, or introduce additional decision criteria during the connection phase. For example, Luo et al. [45] achieved the reconstruction of intricate RSA in challenging environmental conditions through such approaches. Thirdly, developing an automated detection system integrated with GPS positioning and path planning during GPR surveys would minimize human operational errors in field experiments and improve RSA reconstruction accuracy. Fourthly, cross-species validation experiments are crucial for assessing method generalizability, particularly in arboricultural root research. As demonstrated by Latini et al. [46] in reconstructing specific tree root systems using GPR, although arboreal roots exhibit thicker main root systems compared to shrubs, their spatial complexity increases substantially. Related validation experiments could provide new insights for forestry surveys. It should be noted that this study primarily focuses on coarse root system reconstruction in shrubs. Finally, by developing proximal short root attribution recognition and utilizing B-spline curve fitting [47] or employing graph neural networks to encrypt the spatial relationships among multiple short roots [48], the continuity and authenticity of RSA are effectively enhanced.

5. Conclusions

A 'clustering–connection' (CC) method for reconstructing the RSA of coarse roots is proposed. After obtaining the root point cloud data via GPR, the clustering phase considers the aggregation characteristics of the root extension angles. During clustering, the root point cloud data are grouped based on similar root point angles, accounting for the aggregation pattern in the root extension angles. In the connection phase, root growth characteristics are incorporated, and the RSA topology is derived using a threshold limit and MST, ultimately reconstructing the 3D RSA. Experiments with both circular and grid survey lines demonstrate that the CC method is applicable to root point cloud data from various survey line arrangements. The method's accuracy and effectiveness are confirmed through experiments with both simulated and measured data. The experimental results demonstrate that our method effectively extracts root point clusters exhibiting directional aggregation features aligned with root growth trajectories. However, limitations inherent to GPR detection (such as missing root point detections causing uneven spatial distributions) can lead to discontinuous root segments in the reconstructed architecture. Additionally, in field experiments, the complexity of environmental conditions and natural root system morphologies reduces the reconstruction accuracy of our approach. Comparison with existing methods shows that the CC method enhances reconstruction accuracy and makes better use of GPR-acquired root point cloud data.

It is believed that the CC method offers fundamental approaches for using GPR in large-scale plant RSA reconstruction. Due to its non-destructive nature, GPR can be more widely applied in forest-related research. For instance, it can be used to obtain more accurate ecological parameters of root systems, analyze the root distribution of shallow-rooted and deep-rooted plants, and provide insights into the competitive and cooperative relationships between underground root systems.

Author Contributions: Conceptualization, Y.L. and X.C. (Xihong Cui); funding acquisition, X.C. (Xihong Cui); methodology, X.C. (Xihong Cui), X.C. (Xuehong Chen) and X.C. (Xin Cao); supervision, X.C. (Xihong Cui) and X.C. (Xuehong Chen); writing—original draft, Y.L.; writing—review and editing, L.Z., X.C. (Xihong Cui) and H.Y. All authors have read and agreed to the published version of the manuscript.

Funding: This research was funded by National Natural Science Foundation of China, grant number 42271329.

Data Availability Statement: Dataset available on request from the authors.

Acknowledgments: Thanks to the Chenlab team for helping with the experiments!

Conflicts of Interest: The authors declare no conflicts of interest.

Appendix A

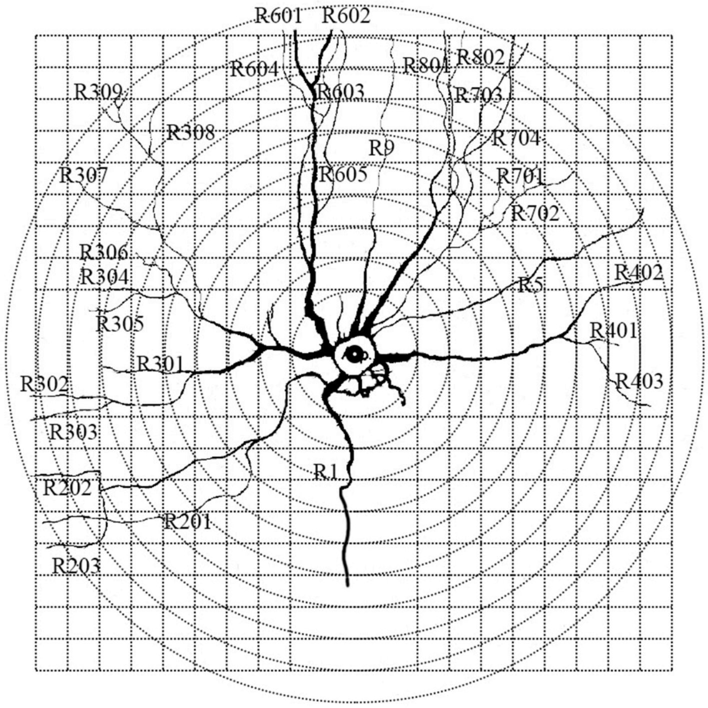

Root bratch number	R1	R201	R202	R203	R301	R302	R303
Depth range(m)	0.2-0.3	0.2-0.4	0.24-0.3	0.28-0.3	0.3-0.35	0.32-0.35	0.33-0.35
Root branch number	R305	R306	R307	R308	R309	R401	R402
Depth range(m)	0.33-0.35	0.33-0.35	0.32-0.36	0.33-0.36	0.35-0.36	0.25-0.3	0.28-0.3
Root branch number	R5	R601	R602	R603	R604	R605	R701
Depth range(m)	0.35-0.5	0.25-0.5	0.42-0.5	0.28-0.3	0.29-0.3	0.31-0.4	0.35-0.4
Root branch number	R703	R704	R801	R802	R9		
Depth range(m)	0.37-0.42	0.37-0.42	0.25-0.3	0.27-0.35	0.35-0.4		

Figure A1. Different root branch numbers and root depth ranges in the simulated data.

References

1. Lambers, H.; Shane, M.W.; Cramer, M.D.; Pearse, S.J.; Veneklaas, E.J. Root Structure and Functioning for Efficient Acquisition of Phosphorus: Matching Morphological and Physiological Traits. *Ann. Bot.* **2006**, *98*, 693–713. [CrossRef] [PubMed]
2. A Starting Guide to Root Ecology: Strengthening Ecological Concepts and Standardising Root Classification, Sampling, Processing and Trait Measurements—Freschet—2021—New Phytologist—Wiley Online Library. Available online: https://nph.onlinelibrary.wiley.com/doi/full/10.1111/nph.17572 (accessed on 18 December 2024).
3. Zhang, Z.; Fan, B.; Song, C.; Zhang, X.; Zhao, Q.; Ye, B. Advances in Root System Architecture: Functionality, Plasticity, and Research Methods. *J. Resour. Ecol.* **2022**, *14*, 15–24. [CrossRef]
4. Maqbool, S.; Hassan, M.A.; Xia, X.; York, L.M.; Rasheed, A.; He, Z. Root System Architecture in Cereals: Progress, Challenges and Perspective. *Plant J.* **2022**, *110*, 23–42. [CrossRef]
5. Atkinson, D. Root Characteristics: Why and What to Measure. In *Root Methods: A Handbook*; Smit, A.L., Bengough, A.G., Engels, C., van Noordwijk, M., Pellerin, S., van de Geijn, S.C., Eds.; Springer: Berlin/Heidelberg, Germany, 2000; pp. 1–32, ISBN 978-3-662-04188-8.
6. Thomas, F.M.; Hartmann, G. Tree Rooting Patterns and Soil Water Relations of Healthy and Damaged Stands of Mature Oak (*Quercus robur* L. and *Quercus petraea* [Matt.] Liebl.). *Plant Soil* **1998**, *203*, 145–158. [CrossRef]
7. Reubens, B.; Poesen, J.; Danjon, F.; Geudens, G.; Muys, B. The Role of Fine and Coarse Roots in Shallow Slope Stability and Soil Erosion Control with a Focus on Root System Architecture: A Review. *Trees* **2007**, *21*, 385–402. [CrossRef]
8. Nakahata, R.; Osawa, A. Fine Root Dynamics after Soil Disturbance Evaluated with a Root Scanner Method. *Plant Soil* **2017**, *419*, 467–487. [CrossRef]
9. Mooney, S.J.; Pridmore, T.P.; Helliwell, J.; Bennett, M.J. Developing X-Ray Computed Tomography to Non-Invasively Image 3-D Root Systems Architecture in Soil. *Plant Soil* **2012**, *352*, 1–22. [CrossRef]

10. Rogers, H.H.; Bottomley, P.A. In Situ Nuclear Magnetic Resonance Imaging of Roots: Influence of Soil Type, Ferromagnetic Particle Content, and Soil Water. *Agron. J.* **1987**, *79*, 957–965. [CrossRef]
11. Van Dusschoten, D.; Metzner, R.; Kochs, J.; Postma, J.A.; Pflugfelder, D.; Bühler, J.; Schurr, U.; Jahnke, S. Quantitative 3D Analysis of Plant Roots Growing in Soil Using Magnetic Resonance Imaging. *Plant Physiol.* **2016**, *170*, 1176–1188. [CrossRef]
12. Todo, C.; Ikeno, H.; Yamase, K.; Tanikawa, T.; Ohashi, M.; Dannoura, M.; Kimura, T.; Hirano, Y. Reconstruction of Conifer Root Systems Mapped with Point Cloud Data Obtained by 3D Laser Scanning Compared with Manual Measurement. *Forests* **2021**, *12*, 1117. [CrossRef]
13. Głuszek, S.; Sas Paszt, L.; Sumorok, B.; Derkowska, E.; Kozera, R. Application of the minirhizotron technique to studying the roots of fruit plants. *Adv. Sci. Technol.-Res. J.* **2013**, *7*, 45–53. [CrossRef]
14. Taylor, B.; Beidler, K.; Strand, A.; Pritchard, S. Improved Scaling of Minirhizotron Data Using an Empirically-Derived Depth of Field and Correcting for the Underestimation of Root Diameters. *Plant Soil* **2013**, *374*, 941–948. [CrossRef]
15. Barton, C.V.M.; Montagu, K.D. Detection of Tree Roots and Determination of Root Diameters by Ground Penetrating Radar under Optimal Conditions. *Tree Physiol.* **2004**, *24*, 1323–1331. [CrossRef] [PubMed]
16. Cui, X.; Chen, J.; Shen, J.; Cao, X.; Chen, X.; Zhu, X. Modeling Tree Root Diameter and Biomass by Ground-Penetrating Radar. *Sci. China Earth Sci.* **2011**, *54*, 711–719. [CrossRef]
17. Cui, X.; Liu, X.; Cao, X.; Fan, B.; Zhang, Z.; Chen, J.; Chen, X.; Lin, H.; Guo, L. Pairing Dual-frequency GPR in Summer and Winter Enhances the Detection and Mapping of Coarse Roots in the Semi-arid Shrubland in China. *Eur. J. Soil Sci.* **2020**, *71*, 236–251. [CrossRef]
18. Resh, S.C.; Battaglia, M.; Worledge, D.; Ladiges, S. Coarse Root Biomass for Eucalypt Plantations in Tasmania, Australia: Sources of Variation and Methods for Assessment. *Trees* **2003**, *17*, 389–399. [CrossRef]
19. Čermák, J.; Hruška, J.; Martinková, M.; Prax, A. Urban Tree Root Systems and Their Survival near Houses Analyzed Using Ground Penetrating Radar and Sap Flow Techniques. *Plant Soil* **2000**, *219*, 103–116. [CrossRef]
20. Hruska, J.; Cermak, J.; Sustek, S. Mapping Tree Root Systems with Ground-Penetrating Radar. *Tree Physiol.* **1999**, *19*, 125–130. [CrossRef]
21. Zou, L.; Wang, Y.; Giannakis, I.; Tosti, F.; Alani, A.M.; Sato, M. Mapping and Assessment of Tree Roots Using Ground Penetrating Radar with Low-Cost GPS. *Remote Sens.* **2020**, *12*, 1300. [CrossRef]
22. Hugenschmidt, J.; Kay, S. Unmasking Adaption of Tree Root Structure in Agroforestry Systems in Switzerland Using GPR. *Geoderma Reg.* **2023**, *34*, e00659. [CrossRef]
23. Wu, Y.; Guo, L.; Cui, X.; Chen, J.; Cao, X.; Lin, H. Ground-Penetrating Radar-Based Automatic Reconstruction of Three-Dimensional Coarse Root System Architecture. *Plant Soil* **2014**, *383*, 155–172. [CrossRef]
24. Ohashi, M.; Ikeno, H.; Sekihara, K.; Tanikawa, T.; Dannoura, M.; Yamase, K.; Todo, C.; Tomita, T.; Hirano, Y. Reconstruction of Root Systems in *Cryptomeria japonica* Using Root Point Coordinates and Diameters. *Planta* **2019**, *249*, 445–455. [CrossRef]
25. Aboudourib, A.; Serhir, M.; Lesselier, D. A Processing Framework for Tree-Root Reconstruction Using Ground-Penetrating Radar Under Heterogeneous Soil Conditions. *IEEE Trans. Geosci. Remote Sens.* **2021**, *59*, 208–219. [CrossRef]
26. Xiao, L.; Li, C.; Cai, Y.; Zhou, M.; Zhou, T.; Gao, X.; Du, H.; Zhou, Y.; Zhou, G. Preliminary Application of Ground-Penetrating Radar for Reconstruction of Root System Architecture in Moso Bamboo. *Remote Sens.* **2021**, *13*, 2816. [CrossRef]
27. Fan, G.; Liang, H.; Zhao, Y.; Li, Y. Automatic Reconstruction of Three-Dimensional Root System Architecture Based on Ground Penetrating Radar. *Comput. Electron. Agric.* **2022**, *197*, 106969. [CrossRef]
28. Luo, W.; Lee, Y.H.; Ow, L.F.; Yusof, M.L.M.; Yucel, A.C. Slice-Relation-Clustering Framework via Horizontal Angle Information for 3-D Tree Roots Reconstruction. *IEEE Trans. Geosci. Remote Sens.* **2023**, *61*, 1–10. [CrossRef]
29. Kummerow, J.; Krause, D.; Jow, W. Root Systems of Chaparral Shrubs. *Oecologia* **1977**, *29*, 163–177. [CrossRef]
30. Guo, L.; Chen, J.; Cui, X.; Fan, B.; Lin, H. Application of Ground Penetrating Radar for Coarse Root Detection and Quantification: A Review. *Plant Soil* **2013**, *362*, 1–23. [CrossRef]
31. Tzanis, A. matGPR Release 2: A Freeware MATLAB® Package for the Analysis & Interpretation of Common and Single Offset GPR Data. *FastTimes* **2010**, *15*, 17–43.
32. Cui, X.; Zhang, Z.; Guo, L.; Liu, X.; Quan, Z.; Cao, X.; Chen, X. The Root-Soil Water Relationship Is Spatially Anisotropic in Shrub-Encroached Grassland in North China: Evidence from GPR Investigation. *Remote Sens.* **2021**, *13*, 1137. [CrossRef]
33. Li, S.; Cui, X.; Guo, L.; Zhang, L.; Chen, X.; Cao, X. Enhanced Automatic Root Recognition and Localization in GPR Images Through a YOLOv4-Based Deep Learning Approach. *IEEE Trans. Geosci. Remote Sens.* **2022**, *60*, 1–14. [CrossRef]
34. Liu, Q.; Cui, X.; Liu, X.; Chen, J.; Chen, X.; Cao, X. Detection of Root Orientation Using Ground-Penetrating Radar. *IEEE Trans. Geosci. Remote Sens.* **2018**, *56*, 93–104. [CrossRef]
35. Dou, Q.; Wei, L.; Magee, D.R.; Cohn, A.G. Real-Time Hyperbola Recognition and Fitting in GPR Data. *IEEE Trans. Geosci. Remote Sens.* **2017**, *55*, 51–62. [CrossRef]
36. Zhang, X.; Xue, F.; Wang, Z.; Wen, J.; Guan, C.; Wang, F.; Han, L.; Ying, N. A Novel Method of Hyperbola Recognition in Ground Penetrating Radar (GPR) B-Scan Image for Tree Roots Detection. *Forests* **2021**, *12*, 1019. [CrossRef]

37. McInnes, L.; Healy, J.; Astels, S. Hdbscan: Hierarchical Density Based Clustering. *J. Open Source Softw.* **2017**, *2*, 205. [CrossRef]
38. Cui, X.; Quan, Z.; Chen, X.; Zhang, Z.; Zhou, J.; Liu, X.; Chen, J.; Cao, X.; Guo, L. GPR-Based Automatic Identification of Root Zones of Influence Using HDBSCAN. *Remote Sens.* **2021**, *13*, 1227. [CrossRef]
39. Wu, Y.; Guo, L.; Li, W.; Cui, X.; Chen, J. Comment on: "Root Orientation Can Affect Detection Accuracy of Ground-Penetrating Radar". *Plant Soil* **2014**, *380*, 441–444. [CrossRef]
40. Luo, W.; Lee, Y.H.; Sun, H.-H.; Ow, G.; Yusof, M.L.M.; Yucel, A.C. Tree Roots Reconstruction Framework for Accurate Positioning in Heterogeneous Soil. *IEEE J. Sel. Top. Appl. Earth Obs. Remote Sens.* **2022**, *15*, 1912–1925. [CrossRef]
41. Zenone, T.; Morelli, G.; Teobaldelli, M.; Fischanger, F.; Matteucci, M.; Sordini, M.; Armani, A.; Ferrè, C.; Chiti, T.; Seufert, G. Preliminary Use of Ground-Penetrating Radar and Electrical Resistivity Tomography to Study Tree Roots in Pine Forests and Poplar Plantations. *Funct. Plant Biol.* **2008**, *35*, 1047. [CrossRef]
42. Hirano, Y.; Yamamoto, R.; Dannoura, M.; Aono, K.; Igarashi, T.; Ishii, M.; Yamase, K.; Makita, N.; Kanazawa, Y. Detection Frequency of *Pinus thunbergii* Roots by Ground-Penetrating Radar Is Related to Root Biomass. *Plant Soil* **2012**, *360*, 363–373. [CrossRef]
43. Cui, X.; Li, S.; Zhang, L. Estimation of Root Diameter in GPR Images via CycleGAN-Guided Multi-Objective Integration Neural Network. In Proceedings of the IGARSS 2024—2024 IEEE International Geoscience and Remote Sensing Symposium, Athens, Greece, 7–12 July 2024; IEEE: Piscataway, NJ, USA, 2024; Volume 15, pp. 6476–6479.
44. Sun, H.-H.; Lee, Y.H.; Dai, Q.; Li, C.; Ow, G.; Yusof, M.L.M.; Yucel, A.C. Estimating Parameters of the Tree Root in Heterogeneous Soil Environments via Mask-Guided Multi-Polarimetric Integration Neural Network. *IEEE Trans. Geosci. Remote Sens.* **2022**, *60*, 1–16. [CrossRef]
45. Luo, W.; Hui Lee, Y.; Hao, T.; Lokman Mohd Yusof, M.; Yucel, A.C. Automatic Dual-Polarized Ground Penetrating Radar for Enhanced 3-D Tree Roots System Architecture Reconstruction. *IEEE Trans. Geosci. Remote Sens.* **2024**, *62*, 1–18. [CrossRef]
46. Lantini, L.; Tosti, F.; Giannakis, I.; Zou, L.; Benedetto, A.; Alani, A.M. An Enhanced Data Processing Framework for Mapping Tree Root Systems Using Ground Penetrating Radar. *Remote Sens.* **2020**, *12*, 3417. [CrossRef]
47. Harmening, C.; Butzer, R. Improving the Approximation Quality of Tensor Product B-Spline Surfaces by Local Parameterization. *J. Appl. Geod.* **2024**, *18*, 575–596. [CrossRef]
48. Lu, Y.; Lu, G. 3D Modeling Beneath Ground: Plant Root Detection and Reconstruction Based on Ground-Penetrating Radar. In Proceedings of the 2022 IEEE/CVF Winter Conference on Applications of Computer Vision (WACV), Waikoloa, HI, USA, 3–8 January 2022; IEEE: Piscataway, NJ, USA; pp. 697–706.